Hindawi Publishing Corporation
Mathematical Problems in Engineering
Volume 2014, Article ID 728950, 7 pages
http://dx.doi.org/10.1155/2014/728950

Research Article

Nonlinear Analysis of Actuation Performance of Shape Memory Alloy Composite Film Based on Silicon Substrate

Shuangshuang Sun[1] and Xiance Jiang[2]

[1] *College of Electromechanical Engineering, Qingdao University of Science & Technology, Qingdao 266061, China*
[2] *Department of Mechanical and Aeronautical Engineering, Naval Aeronautical Engineering Academy Qingdao Branch, Qingdao 266041, China*

Correspondence should be addressed to Shuangshuang Sun; sunkira@sohu.com

Received 25 September 2013; Revised 24 January 2014; Accepted 12 February 2014; Published 20 March 2014

Academic Editor: Mahmoud Kadkhodaei

The mechanical model of the shape memory alloy (SMA) composite film with silicon (Si) substrate was established by the method of mechanics of composite materials. The coupled action between the SMA film and Si substrate under thermal loads was analyzed by combining static equilibrium equations, geometric equations, and physical equations. The material nonlinearity of SMA and the geometric nonlinearity of bending deformation were both considered. By simulating and analyzing the actuation performance of the SMA composite film during one cooling-heating thermal cycle, it is found that the final cooling temperature, boundary condition, and the thickness of SMA film have significant effects on the actuation performance of the SMA composite film. Besides, the maximum deflection of the SMA composite film is affected obviously by the geometric nonlinearity of bending deformation when the thickness of SMA film is very large.

1. Introduction

Microactuators are key parts for microactuating in micro-electro-mechanical systems (MEMS). Compared with other microactuators, bimorph thin film SMA microactuators composed of thin film SMAs and Si substrates have been paid much more attention recently [1–3] due to the simple structure, large work density, and rapid response. Some prototypes of bimorph thin film SMA microactuators have been fabricated, for instance, microvalves, micropumps, microgrippers, and so forth. The review of the SMA/Si composite film used as microactuators in MEMS can be made to the references of Ning et al. [4] and Fu et al. [5, 6].

To make SMA/Si composite film be used as good-performance and high-efficient microactuators in MEMS and also to reduce the cost of research and development, predicting and analyzing the actuation performance of SMA/Si composite film theoretically are very necessary. A few researchers have done some work in this aspect. For example, Wang [7] studied the actuating performance of SMA/Si composite film by the bimetal theory [8] for linear-elastic materials. But the theoretical result is about four times of that of tests. Cheng [9] made some optimization research on the dynamic actuation characteristics of TiNi(Cu)/Si composite diaphragm by the commercial software ANSYS and gave some qualitative comparison with experiments. Wang et al. [10] simulated the actuation displacements of a Si/TiNi bimorph structure by ANSYS and compared them with test results, yet larger differences exist between them. It is noted that these simulations by ANSYS were all based on geometric linear analysis and the nonlinear physical relation of SMA was input by discrete data. Authors in [11] have made some preliminary studies on the modeling and actuation characteristics of NiTi/Si composite film by the method of mechanics of materials, but only the material nonlinearity of SMA was considered. Generally the actual thickness of the SMA/Si composite film used as microactuators is very small with sizes from a few micrometers to dozens of micrometers. But the largest bending displacement of SMA composite film along thickness is usually approach to or much larger than the size of thickness during working, which produces the geometric nonlinearity of bending deformation. So the effects of geometric nonlinearity of deformation on the actuation performance of SMA/Si composite film should be considered

when modeling and predicting. Yet little work was reported in this aspect.

We have done some work [12] on the actuation performance of NiTi/Si composite film by considering both the material nonlinearity of SMA and the geometric nonlinearity of bending deformation, yet only the maximum actuation displacement of simply-supported NiTi/Si composite film varying with three final cooling temperatures and the maximum actuation displacement of cantilever NiTi/Si composite film varying with SMA thickness were studied. As for the relations between the maximum actuation displacement and the phase transformation fraction and stress of SMA during thermal cycles, they were not of concern. Additionally how boundary conditions affect the actuation performance of NiTi/Si composite film was not discussed theoretically and numerically. Based on our previous work [11, 12], the SMA/Si composite film will be further studied in this paper to comprehensively predict its actuation performance by considering both the material nonlinearity of SMA and the geometric nonlinearity of bending deformation. The SMA/Si composite film subjected to thermal loads will be modeled according to the method of mechanics of composite materials. The effects of the final cooling temperature, boundary condition, thickness of SMA film, and geometric nonlinearity of deformation on the actuation performance of SMA/Si composite film will be discussed in detail. The influence of the phase transformation fraction and stress of SMA on the maximum actuation displacement of SMA/Si composite film will also be explored.

2. Modeling of SMA/Si Composite Film

The SMA/Si composite film is considered as a composite beam in this paper. Figure 1(a) shows the schematic diagram of an SMA/Si composite film element before working, where t_a and t_m denote the thickness of the SMA film and Si substrate, respectively. Figure 1(b) shows the working state of a microsegment of the SMA composite film element under thermal loads, where M is the bending moment in each cross-section of the SMA composite film and $d\theta$ is the relative rotation angle of the left and the right cross-sections of the microsegment with length dx.

To analyze the actuation performance of the SMA composite film under thermal loads, the coordinate system is established as shown in Figure 1(a). The coupled action between the SMA film and the Si substrate will be analyzed by combining static equilibrium equations, geometric equations, and physical equations in the following sections.

2.1. Static Equilibrium Equations. Because no mechanical loads are applied on the SMA/Si composite film except for thermal loads, the following static equilibrium equations [13] must be satisfied for the microsegment in Figure 1(b):

$$F_x = \int_0^{t_m} \sigma_m \cdot b \cdot dy + \sigma_a \cdot b \cdot t_a = 0,$$
$$M_{xz} = \int_0^{t_m} \sigma_m \cdot y \cdot b \cdot dy + \sigma_a \cdot y_a \cdot b \cdot t_a \cong M, \quad (1)$$

where F_x and M_{xz} denote resultant internal forces and internal moments in each cross-section of the microsegment in Figure 1(b). σ_m and σ_a denote the stress of Si substrate and the SMA film, respectively. b is the width of the SMA composite film. y_a is the transverse coordinate of the midheight of SMA film with $y_a = -t_a/2$. The bending moment M has the approximate expression [11] of $M = \sigma_a t_a b(t_m + t_a)/2$. Note that the stress of SMA is considered to have no change of gradient along its thickness as the thickness of SMA is usually smaller than that of Si substrate.

2.2. Geometric Equations. Assume the curvature radius and strain of the interface in the SMA composite beam to be ρ_0 and ε_0. From the geometric relation shown in Figure 1, we have the following expression:

$$\varepsilon_0 = \rho_0 \left(\frac{d\theta}{dx}\right) - 1 = \rho_0 k_0 - 1, \quad (2)$$

where, $k_0 = d\theta/dx$.

Then the strain ε_m of an arbitrary fiber bb with the distance y to the interface in Si substrate can be expressed as

$$\varepsilon_m = \varepsilon_0 + k_0 y. \quad (3)$$

For the SMA film, the strain ε_a of any points is assumed to be equal with the following approximate expression:

$$\varepsilon_a = \varepsilon_0 + k_0 \left(-\frac{t_a}{2}\right). \quad (4)$$

And the curvature k of the midplane of the SMA composite film can be written as

$$k = \frac{1}{\left[\rho_0 + \left(\left(t_a + t_m\right)/2 - t_a\right)\right]}. \quad (5)$$

2.3. Physical Equations. Assume that the constitutive relation of Si substrate is linear elastic though geometrically nonlinear deformation will occur in the SMA/Si composite film during working. Then the stress-strain relationship of Si substrate under thermal loads can be written as

$$\sigma_m = \left(\varepsilon_m - \alpha_m \cdot \Delta T\right) \cdot E_m, \quad (6)$$

where, σ_m, α_m, and E_m denote the stress, thermal expansion coefficient, and elastic modulus of Si substrate, respectively. ΔT is the change of temperature.

For the SMA film, the Liang-Rogers' constitutive model [14] modified by Wang [7] is employed in the following:

$$\sigma_a = D(\xi)\varepsilon_a + \Omega(\xi)\xi + \theta(\xi)T + S_0, \quad (7)$$

where $S_0 = \sigma_{a0} - D(\xi_0)\varepsilon_{a0} - \Omega(\xi_0)\xi_0 - \theta(\xi_0)T_0$. D, Ω, and θ denote the elastic modulus, phase transformation modulus and thermal elastic modulus of SMA, respectively. They are all the functions of martensite fraction ξ. T represents temperature. The quantities with the subscript 0 denote initial conditions. In addition, we have three expressions $D(\xi) = D_A + \xi(D_M - D_A)$, $\Omega(\xi) = -\varepsilon_L D(\xi)$, and $\theta(\xi) = -\alpha D(\xi)$. Here D_A and D_M are the austenite and martensite elastic modulus, ε_L is the maximum residual strain, and α is the thermal expansion coefficient of SMA.

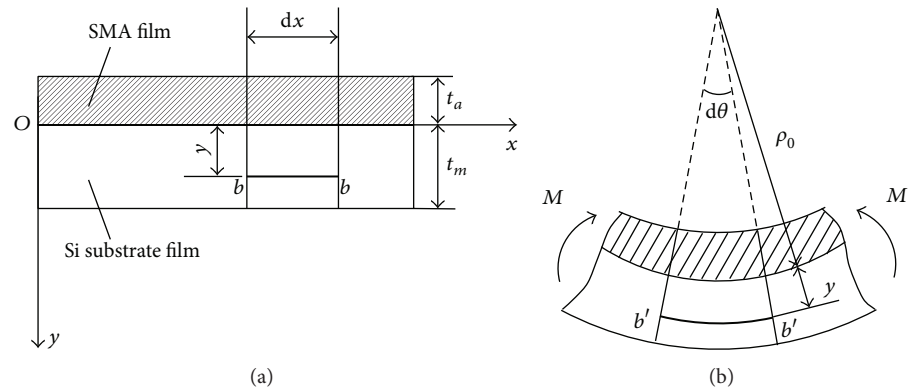

FIGURE 1: Schematic diagram of the SMA/Si composite film element (a) before thermal loads are applied and (b) microsegment after thermal loads are applied.

2.4. Phase Transformation Equations of SMA. When SMA undergoes phase transformations, the following phase transformation kinetics proposed by Liang-Rogers [14] are employed.

Conversion from martensite to austenite for $C_A(T-A_f) < \sigma_a < C_A(T-A_s)$:

$$\xi = \frac{\xi_0}{2}\left\{\cos\left[a_A\left(T-A_s\right)+b_A\sigma_a\right]+1\right\}. \tag{8}$$

Conversion from austenite to martensite for $C_M(T-M_s) < \sigma_a < C_M(T-M_f)$:

$$\xi = \frac{\left(1-\xi_0\right)}{2}\cos\left[a_M\left(T-M_f\right)+b_M\sigma_a\right]+\frac{\left(1+\xi_0\right)}{2}. \tag{9}$$

In (8) and (9), a_A, a_M, b_A, and b_M are material constants of SMA with the relationship $a_A = \pi/(A_f - A_s)$, $a_M = \pi/(M_S - M_f)$, $b_A = -a_A/C_A$, and $b_M = -a_M/C_M$. Additionally M_S, M_f, A_s, and A_f denote the martensite start, martensite finish, austenite start, and austenite finish temperatures of SMA in the stress-free state, respectively. C_A and C_M are material parameters that describe the relationship of temperature and the critical stress to induce transformations.

Combining (1)–(7), we get the following three expressions:

$$\sigma_a = \frac{\alpha_m\Delta T-\left(\varepsilon_L\xi+\alpha T\right)+S_0/D\left(\xi\right)}{1/D\left(\xi\right)+\left[t_a\left(7t_m^2+12t_at_m+6t_a^2\right)\right]/\left(E_mt_m^3\right)}, \tag{10}$$

$$\varepsilon_0 = \alpha_m\cdot\Delta T-\frac{\sigma_a\cdot t_a\left(7t_m+6t_a\right)}{E_m\cdot t_m^2}, \tag{11}$$

$$k_0 = \frac{12\sigma_a\cdot t_a\left(t_m+t_a\right)}{E_m\cdot t_m^3}. \tag{12}$$

Note that (10) is a nonlinear equation when phase transformations occurs in SMA, as σ_a, ξ, and T are coupled together. If the phase transformation is from martensite to austenite, then σ_a can be obtained by solving (10) and (8) by using the subroutine ZREAL given in Visual Fortran. If the phase transformation is from austenite to martensite, then σ_a can be obtained by solving (10) and (9) by using the same subroutine. But if there are no phase transformations in SMA, ξ is always a constant. Then (10) is a linear equation about σ_a and T. The current stress of SMA corresponding to the current temperature can be directly obtained by solving this equation.

Once σ_a is obtained, then ε_0 and k_0 can be calculated out from (11) and (12), respectively. And the curvature k of the midplane can be obtained from (5).

3. Bending Deformation of SMA/Si Composite Film

The maximum displacement produced in working is an important index of weighting the actuation capability of SMA/Si composite film. In this section, the maximum deflection (i.e., displacement of centroid in each cross-section along the thickness direction) expressions of SMA/Si composite film will be derived for two common boundary conditions: both ends are simply supported (S-S), and one end is fixed and the other is free (F-F).

The general expression of the deflection equation of SMA/Si composite film can be written as

$$\frac{\mathrm{d}^2w/\mathrm{d}x^2}{\left[1+\left(\mathrm{d}w/\mathrm{d}x\right)^2\right]^{3/2}} = k, \tag{13}$$

where w denotes the deflection of SMA/Si composite film. It is defined to be positive along the positive y-axis direction shown in Figure 1.

In the case of small deformations, (13) can be simplified as the following linear differential equation:

$$\frac{\mathrm{d}^2w}{\mathrm{d}x^2} = k. \tag{14}$$

Solving the differential equations of (13) and (14) by combining boundary conditions, we get the following expressions of the maximum deflection of SMA composite film.

Table 1: Material properties of NiTi-SMA and Si [7].

NiTi SMA	$M_f = 23^\circ\text{C}$	$C_M = 11.3\,\text{MPa}/^\circ\text{C}$
	$M_s = 50^\circ\text{C}$	$C_A = 4.5\,\text{MPa}/^\circ\text{C}$
	$A_s = 62^\circ\text{C}$	$D_M = 13\,\text{GPa}$
	$A_f = 100^\circ\text{C}$	$D_A = 30\,\text{GPa}$
	$\alpha = 8.8 \times 10^{-6}/^\circ\text{C}$	$\varepsilon_L = 1\%$
Si	$E_m = 180.5\,\text{GPa}$	$\alpha_m = 2.33 \times 10^{-6}/^\circ\text{C}$

Under S-S boundary condition

$$w_{\max}^N = \frac{1}{k} - \frac{1}{k}\sqrt{1 - \left(\frac{L \cdot k}{2}\right)^2}, \qquad w_{\max}^L = \frac{1}{8}kL^2. \tag{15}$$

Under F-F boundary condition

$$w_{\max}^N = -\frac{1}{k} + \frac{1}{k}\sqrt{1 - (kL)^2}, \qquad w_{\max}^L = -\frac{1}{2}kL^2, \tag{16}$$

where $w_{\max}^N$ and $w_{\max}^L$ represent the maximum deflections obtained from the nonlinear differential equation of (13) and the linear differential equation of (14), respectively. L denotes the total length of the SMA/Si composite film.

4. Numerical Simulation and Discussions

In this section, the actuation performance of the NiTi-SMA composite film with Si substrate in a cooling-heating thermal cycle will be simulated and discussed. The NiTi-SMA composite film is cooled first from the crystallization temperature T_{cry} (550°C) to the final cooling temperature T_f and then it is heated from T_f to T_{cry} again.

Material parameters of NiTi-SMA and Si used in simulation are taken from Wang [7] and shown in Table 1. Unless otherwise specified, the geometric sizes of the SMA composite film are $t_a = 5\,\mu$m, $t_m = 20\,\mu$m, and $L = 3$ mm. The boundary condition is S-S. The initial stress and strain of NiTi SMA at T_{cry} are zero. $T_f = 30^\circ$C. The simulation results are given in Figures 2–4.

To observe the influence of the final cooling temperature T_f on actuation performance of SMA composite film, the SMA composite film at T_{cry} are firstly cooled to 30°C, 40°C, and 50°C, respectively and then heated to T_{cry} again. In the three cooling-heating thermal cycles, the maximum deflection $w_{\max}^N$ of SMA composite film, martensite fraction ξ, and stress σ_a of SMA varying with temperature are given in Figures 2(a), 2(b), and 2(c), respectively.

From Figure 2(a) we can see that $w_{\max}^N$ increases first with decreasing temperature during cooling due to the action of thermal stresses produced between SMA and Si substrate, then it decreases rapidly with decreasing temperature when SMA undergoes phase transformation from austenite to martensite for each case of T_f. In addition, the lower the value of T_f is, the more obviously the value of $w_{\max}^N$ decreases. This is because that more austenite transforms to martensite at lower T_f (see Figure 2(b)). For $T_f = 30^\circ$C, $w_{\max}^N$ decreases to zero at about 40°C during cooling and then it continues to decrease to some negative value with the ongoing decreasing of temperature. During heating, $w_{\max}^N$ for each case of T_f has a slight change first and then its value increases rapidly with increasing temperature once reverse phase transformation from martensite to austenite occurs in SMA. When SMA ends reverse phase transformation, the value of $w_{\max}^N$ decreases again with increasing temperature due to thermal stress between SMA and Si substrate. It recovers to zero again when temperature is raised to T_{cry}.

Figure 2(b) shows martensite fraction of SMA varying with temperature during the three cooling-heating thermal cycles. It can be seen from this figure that martensite fraction increases rapidly from zero with the decreasing of temperature during cooling when SMA undergoes phase transformation from austenite to martensite. And the lower the value of T_f is, the larger the martensite fraction is at the end of cooling. For instance, the martensite fraction is about 0.81 for $T_f = 30^\circ$C. And it is about 0.07 for $T_f = 50^\circ$C. While martensite fraction decreases rapidly with increasing temperature during heating when reverse phase transformation occurs in SMA. When temperature is raised to T_{cry}, all martensite is completely transformed into austenite.

Figure 2(c) illustrates the variation of SMA stress with temperature during the three cooling-heating thermal cycles. We can see that the stress of SMA reaches very high value before phase transformation occurs in SMA during the cooling stage for each case of T_f. This is induced by the bimetal effect between SMA and Si substrate. But the stress of SMA decreases dramatically with temperature once SMA undergoes phase transformation from austenite to martensite during the ongoing cooling stage. For $T_f = 30^\circ$C, the maximum tensile stress of SMA is decreased with the largest amplitude, which decreases to zero first at about 40°C and then continues to decrease to negative values. The stress of SMA increases dramatically when reverse phase transformation occurs in SMA during the heating stage, and it becomes zero again when temperature reaches T_{cry}.

In summary, Figures 2(a), 2(b), and 2(c) tell us that thermal stresses produced between SMA and Si during cooling can be released completely by the shape memory effect of SMA. And the maximum deflection of the NiTi-SMA composite film induced by thermal stresses can also be recovered completely, if T_f is properly set during cooling. This is very important for the design of bimorph thin film SMA microactuators.

The maximum deflections $w_{\max}^N$ varying with temperature for SMA composite films under S-S and F-F boundary conditions are given in Figure 3 to observe effects of different boundary conditions during the cooling-heating thermal cycle.

It can be seen from Figure 3 that boundary conditions have significant effects on the maximum deflection of SMA composite film. Under S-S boundary condition, the maximum deflection keeps approximately all positive values during the cooling-heating thermal cycle. While most part of the maximum deflection of SMA composite film keeps negative values under F-F boundary condition. Additionally

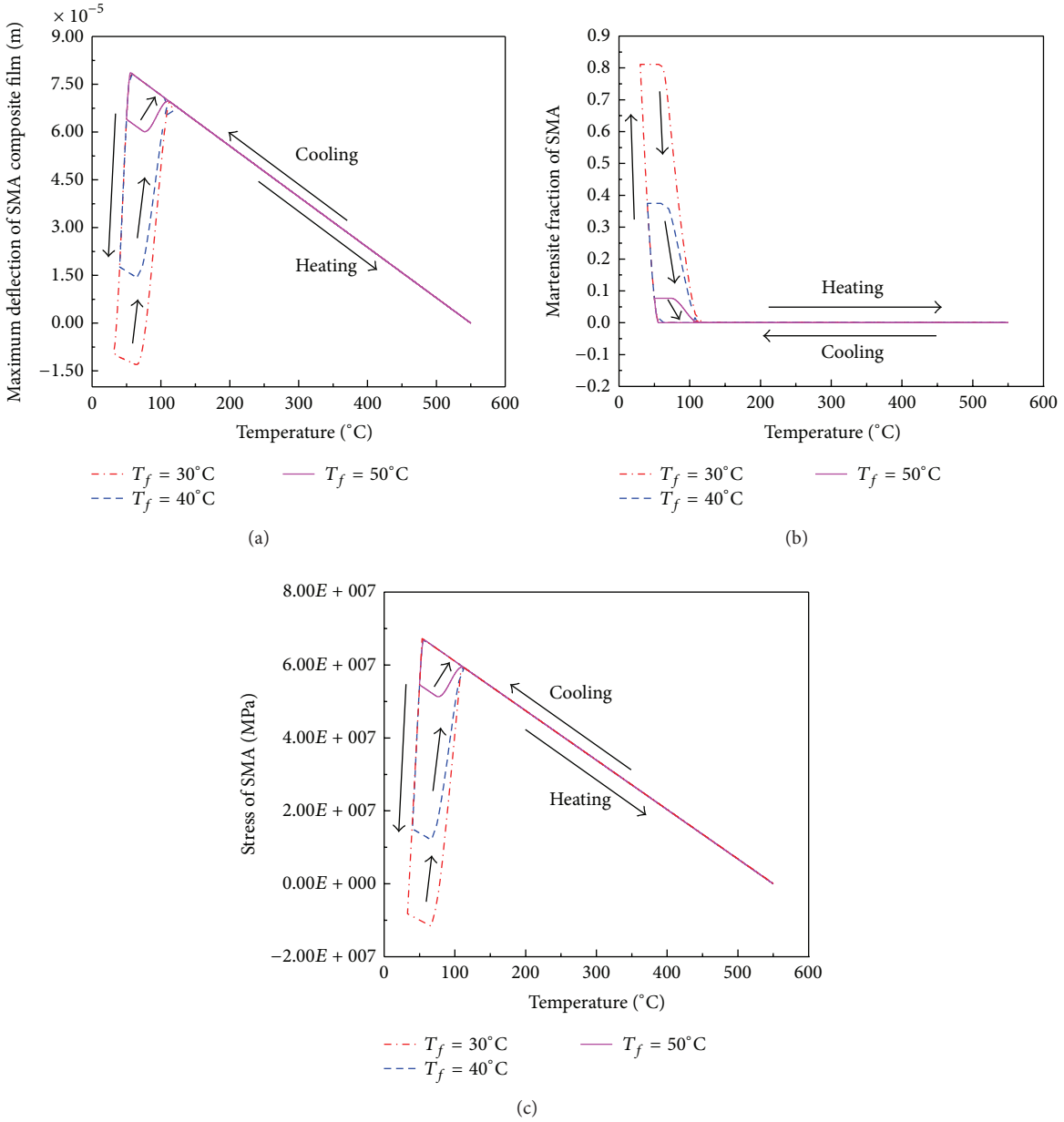

FIGURE 2: Effects of the final cooling temperature T_f on SMA composite film (a) the maximum deflection of SMA composite film varying with temperature, (b) the martensite fraction of SMA varying with temperature, and (c) the stress of SMA varying with temperature.

the largest absolute value of the maximum deflection under F-F boundary condition is more than four times of that under S-S boundary condition during the whole thermal cycle. This results from higher thermal stresses produced in SMA composite film under F-F boundary condition. We also can see from Figure 3 that the largest absolute value of the maximum deflection under each boundary condition recovers fully to zero first and then increases slightly to the reverse direction when SMA undergoes phase transformation from austenite to martensite. And the absolute value of the maximum deflection under each boundary condition increases dramatically once the reverse phase transformation occurs in SMA. It begins to decrease slowly after the reverse phase transformation is finished during the ongoing heating stage.

Figures 4(a) and 4(b) show effects of SMA thickness on the maximum deflection of SMA composite film under F-F and S-S boundary conditions, respectively. Both $w^N_{\max}$ and $w^L_{\max}$ are given in the two figures to observe influence of the geometric nonlinearity of bending deformation.

From Figure 4 we can see that the maximum deflections of $w^N_{\max}$ and $w^L_{\max}$ increase with the increasing of the SMA thickness. This is probably due to the fact that the SMA/Si composite film will produce higher thermal stresses when the SMA film is thicker. But $w^L_{\max}$ is always smaller than $w^N_{\max}$ for each SMA thickness under each boundary condition.

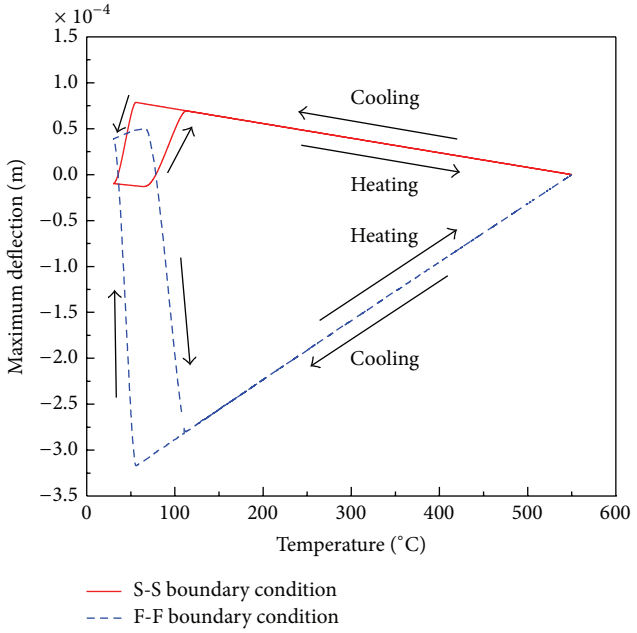

FIGURE 3: Effects of boundary conditions on the maximum deflection of SMA composite film.

In addition, the difference between $w_{\max}^{N}$ and $w_{\max}^{L}$ becomes more obvious when the thickness of SMA film becomes larger especially under F-F boundary condition. This demonstrates that the geometric nonlinearity of bending deformation should be considered when the thickness of SMA film is very large.

5. Conclusions

The mechanical model of the SMA composite film with Si substrate was established by the method of mechanics of composite materials in this paper. The actuation performance of the SMA/Si composite film subjected to thermal loads was simulated and analyzed during one cooling-heating thermal cycle. The effects of the final cooling temperature, boundary condition, SMA thickness, and geometric nonlinearity on the actuation performance of the NiTi-SMA composite film were discussed. The following conclusions can be drawn from the present study.

(1) The maximum deflection produced by thermal stresses recovers more obviously when more austenite transforms to martensite during cooling for SMA/Si composite film with lower T_f.

(2) The maximum actuation displacement along thickness under F-F boundary condition is more than four times of that under S-S boundary condition for SMA/Si composite film during one cooling-heating thermal cycle.

(3) The maximum deflection of SMA/Si composite film increases with increasing the thickness of SMA film whether under F-F boundary condition or under S-S boundary condition.

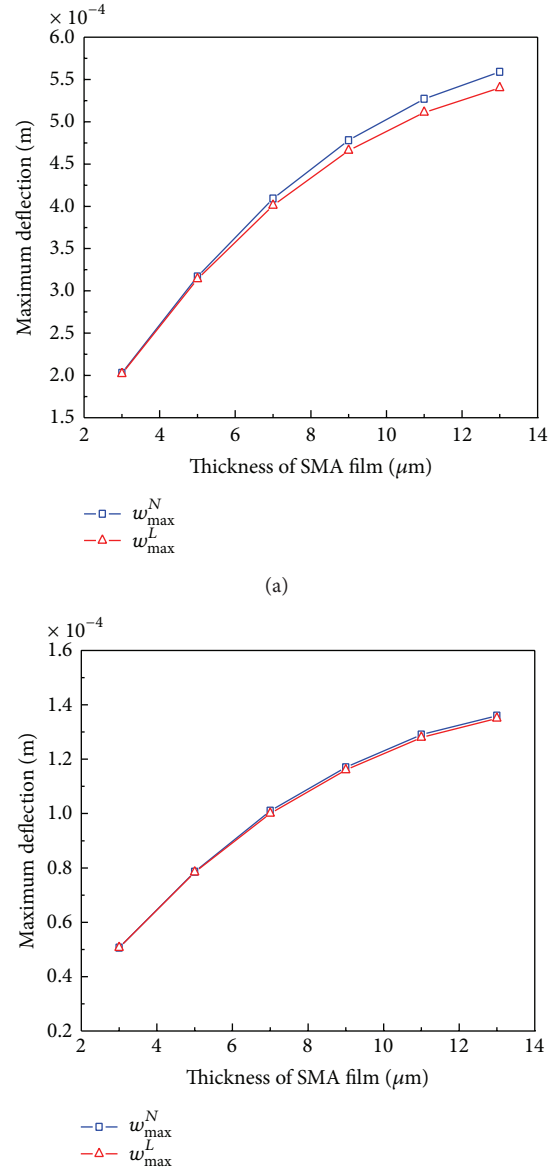

FIGURE 4: Effects of SMA thickness on the maximum deflection of SMA composite film (a) F-F boundary condition and (b) S-S boundary condition.

(4) Effects of geometric nonlinearity of bending deformation on the actuation displacement of SMA/Si composite film becomes more obvious when the thickness of SMA film becomes larger especially under F-F boundary condition.

This study can provide some helpful guidance for the design and application of bimorph thin film SMA microactuators in MEMS.

Conflict of Interests

The authors declare that there is no conflict of interests regarding the publication of this paper.

Acknowledgments

The authors acknowledge the financial support of the Promotive Research Fund for Excellent Young and Middle-aged Scientists of Shandong Province (no. BS2010CL016), the Project of Shandong Province Higher Educational Science and Technology Program (no. J13LB08), and the Project of Science and Technology Development Plan of Qingdao (no. 13-1-4-150-jch).

References

[1] D. Xu, L. Wang, G. Ding, Y. Zhou, A. Yu, and B. Cai, "Characteristics and fabrication of NiTi/Si diaphragm micropump," *Sensors and Actuators A: Physical*, vol. 93, no. 1, pp. 87–92, 2001.

[2] J. Teng and P. D. Prewett, "Focused ion beam fabrication of thermally actuated bimorph cantilevers," *Sensors and Actuators A: Physical*, vol. 123-124, pp. 608–613, 2005.

[3] J. H. Cao, B. L. Wang, C. Ye, and H. Wang, "Micropump design based on NiTi shape memory alloy," *Science &Technology Information*, vol. 29, pp. 548–549, 2011.

[4] Z. H. Ning, Z. G. Wang, Y. Q. Fu, and X. T. Zu, "Advances of investigation on TiNi-based shape memory alloy films," *Materials Review*, vol. 20, no. 2, pp. 118–125, 2006.

[5] Y. Q. Fu, H. J. Du, W. M. Huang, S. Zhang, and M. Hu, "TiNi-based thin films in MEMS applications: a review," *Sensors and Actuators A: Physical*, vol. 112, no. 2-3, pp. 395–408, 2004.

[6] Y. Q. Fu, J. K. Luo, A. J. Flewitt, W. M. Huang, and W. I. Milne, "Thin film shape memory alloys and microactuators," *International Journal of Computational Materials Science and Surface Engineering*, vol. 2, no. 3-4, pp. 209–226, 2009.

[7] L. Wang, *Theory and techniques of thin film shape memory alloy microactuators based on silicon substrate [Ph.D. thesis]*, Shanghai Jiaotong University, 2000.

[8] S. Timoshenko and J. Gere, *Mechanics of Materials*, Van Nostrand Reinhold, New York, NY, USA, 1972.

[9] X. L. Cheng, *Optimization research of dynamic actuating characteristics of TiNi(Cu)/Si composite diaphragm based on MEMS technology [Ph.D. thesis]*, Shanghai Jiaotong University, 2002.

[10] Y. P. Wang, Y. B. Wu, X. B. Zhang, C. C. Zhang, and C. S. Yang, "Simulation and fabrication of an SMA electro-thermal actuator with Si/ TiNi bimorph structure," *Micronanoelectronic Technology*, vol. 47, no. 2, pp. 93–98, 2010.

[11] S. S. Sun and J. Dong, "Modeling and simulation on the actuation performance of shape memory alloy/Si composite diaphragm," *Journal of Shanghai Jiaotong University*, vol. 44, no. 8, pp. 1145–1149, 2010.

[12] S. S. Sun and X. C. Jiang, "Nonlinear analysis of actuation performance of NiTi/Si composite film," *Applied Mechanics and Materials*, vol. 437, pp. 572–576, 2013.

[13] G. L. Shen and G. K. Hu, *Mechanics of Composite Materials*, Publishing House of Tsinghua University, Beijing, China, 2006.

[14] C. Liang and C. A. Rogers, "One-dimensional thermomechanical constitutive relations for shape memory materials," *Journal of Intelligent Material Systems and Structures*, vol. 8, no. 4, pp. 285–302, 1997.